Optomechanically induced transparency

S. Weis[1,2,†], R. Rivière[2,†], S. Deléglise[1,2,†], E. Gavartin[1], O. Arcizet[3], A. Schliesser[1,2], T. J. Kippenberg[1*]

[1]*Ecole Polytechnique Fédérale de Lausanne, EPFL, 1015 Lausanne, Switzerland,*
[2]*Max-Planck-Institut für Quantenoptik, Hans-Kopfermann-Str. 1, 85748 Garching, Germany,*
[3]*Institut Néél, 25 rue des Martyrs, 38042 Grenoble, France and*
[†]*These authors contributed equally to this work.*

Coherent interaction of laser radiation with multilevel atoms and molecules can lead to quantum interference in the electronic excitation pathways [1]. A prominent example observed in atomic three-level-systems is the phenomenon of electromagnetically induced transparency (EIT), in which a control laser induces a narrow spectral transparency window for a weak probe laser beam [2]. The concomitant rapid variation of the refractive index in this spectral window can give rise to dramatic reduction of the group velocity of a propagating pulse of probe light [3, 4]. Dynamic control of EIT via the control laser enables even a complete stop, that is, storage, of probe light pulses in the atomic medium [5, 6]. Here, we demonstrate *optomechanically induced transparency* (OMIT)–formally equivalent to EIT–in a cavity optomechanical system operating in the resolved sideband regime [7–9]. A control laser tuned to the lower motional sideband of the cavity resonance induces a dipole-like interaction of optical and mechanical degrees of freedom [10–12]. Under these conditions, the destructive interference of excitation pathways for an intracavity probe field gives rise to a window of transparency when a two-photon resonance condition is met. As a salient feature of EIT, the power of the control laser determines the width and depth of the probe transparency window. OMIT could therefore provide a new approach for delaying, slowing and storing light pulses [7, 8, 13] in long-lived mechanical excitations of optomechanical systems, whose optical and mechanical properties can be tailored in almost arbitrary ways in the micro- [14–16] and nano-optomechanical [17–21] platforms developed to date [22].

When the generic EIT effect has first been observed in an atomic gas [23], its great application potential in non-linear optics and optical (quantum) information processing was quickly recognized. In this context, the experimental demonstration of slowing and stopping light [3–6] has particularly attracted researchers' attention, as it provides a route to implement a photonic quantum memory [24] or a classical optical buffer. EIT has

subsequently been studied in a wide variety of atomic media, but also in a number of solid-state systems [25–27] with a well-suited level structure. More recently, a wider class of physical systems, which can be more flexibly engineered—such as coupled plasmonic [28] or optical resonators [29, 30]—have been reported to display a related effect often referred to as coupled-resonantor induced transparency (CRIT) [31]. While CRIT bears some conceptual analogies to atomic EIT, the coupling of the involved resonators and the resulting transparency is usually not induced by an electromagnetic field, but is rather determined by the geometry of the structure, and therefore more difficult to tune.

Recent experiments with optomechanical systems have demonstrated that the *mechanical* response to thermal forces can be controlled by an optical field. This effect has been exploited, for example, to implement optomechanical laser cooling and amplification [14, 32–34], strong optomechanical coupling [16], and optical spring-tuning of coupled mechanical resonances [35]. It was recently suggested [7, 8] to employ optomechanical coupling to control the system's *optical* response to a weak 'probe' laser by a second, 'control' laser driving the lower motional sideband. As pointed out also by an independent study [9], this effect can be considered a strict optomechanical analog of EIT. Advantageously, this form of induced transparency does not rely on naturally occuring resonances and could therefore also be applied to previously inaccesible wavelength regions such as the technologically important near-infrared. Furthermore, already a single optomechanical element can achieve unity contrast, which in the atomic case is only possible within the setting of cavity QED [36]. In this letter we present the first experimental observation of this effect.

The basic idea of our experiment is illustrated in figure 1. It consists of a canonical optomechanical system that features linear optomechanical coupling in the sense that the displacement x of a mechanical mode shifts the cavity resonance frequency to a new frequency $\omega_c' = \omega_c + g_0 x$ with $g_0 \equiv d\omega_c'/dx$. A control laser (frequency ω_l) maintains a control field $\bar{a}e^{-i\omega_l t}$, containing $|\bar{a}|^2$ photons, in the cavity. The static radiation pressure originating from this field displaces the mechanical mode by $\bar{x}$, leading to an effective detuning from the cavity resonance given by $\bar{\Delta} = \omega_l - (\omega_c + g_0\bar{x})$. Here we consider the situation where the control laser is tuned close to the lower motional sideband, i.e. $\bar{\Delta} \approx -\Omega_m$. A second, weak laser oscillating at $\omega_p = \omega_l + \Omega$, is subsequently used to probe

the (modified) cavity resonance by driving an intracavity probe field contained in a perturbation term $\delta a(t)$.

In the case of a weak probe field (compared to the control field), it is straightforward to treat this scenario by linearizing the optomechanical dynamics [37, 38] for the mechanical displacement $x(t) = \bar{x} + \delta x(t)$ and the intracavity field $a(t) = (\bar{a} + \delta a(t))e^{-i\omega_l t}$ around the steady state values $(\bar{x}, \bar{a})$. For the probe power transmission—that is, the ratio of the probe power returned from the system divided by the input probe power—the general expression

$$|t_{\mathrm{p}}|^2 = \left| 1 - \frac{1 + if(\Omega)}{-i(\bar{\Delta} + \Omega) + \kappa/2 + 2\bar{\Delta}f(\Omega)} \eta_{\mathrm{c}}\kappa \right|^2 \quad (1)$$

with

$$f(\Omega) = \hbar g_0^2 \bar{a}^2 \frac{\chi(\Omega)}{i(\bar{\Delta} - \Omega) + \kappa/2}. \quad (2)$$

can be derived (see refs. [7–9] and the appendix). Here, $\chi(\Omega) = (m_{\mathrm{eff}}(\Omega_{\mathrm{m}}^2 - \Omega^2 - i\Gamma_{\mathrm{m}}\Omega))^{-1}$ is the susceptibility of the mechanical oscillator of effective mass m_{eff}, resonance frequency Ω_{m} and damping rate Γ_{m}. The optical mode is characterized by a total loss rate $\kappa = \kappa_0 + \kappa_{\mathrm{ex}}$ and the cavity coupling parameter $\eta_{\mathrm{c}} = \kappa_{\mathrm{ex}}/(\kappa_0 + \kappa_{\mathrm{ex}})$. As shown in figure 1, the presence of a control field $\bar{a}$ induces a transmission window for the probe beam when the resonance condition $\Omega \approx \Omega_{\mathrm{m}}$ is met. The depth and the width of this transmission window are tunable by the power of the control beam as expected from the analogy with EIT.

In order to gain more *physical* insight into how this effect arises, it is instructive to consider the occurring processes in a sideband picture. The simultaneous presence of control and probe fields generates a radiation-pressure force oscillating at the frequency difference Ω of the two fields. If this driving force oscillates close to the mechanical resonance frequency Ω_{m}, the mechanical mode starts to oscillate coherently, $\delta x(t) = 2\mathrm{Re}[X e^{-i\Omega t}]$, where X denotes the (complex) oscillation amplitude. This in turn gives rise to Stokes- and anti-Stokes scattering of light from the strong intracavity control field. If the system resides deep enough in the resolved-sideband (RSB) regime with $\kappa \ll \Omega_{\mathrm{m}}$, Stokes scattering (to the optical frequency $\omega_l - \Omega$) is strongly suppressed since it is highly off-resonant with the optical cavity. We can therefore assume that only an anti-Stokes field builds up inside the cavity, $\delta a(t) \approx A^- e^{-i\Omega t}$. However, the anti-Stokes scattered light exhibits the frequency $\omega_{\mathrm{p}} = \omega_l + \Omega$; it is degenerate with the near-resonant probe field sent to the cavity. Destructive interference of these two driving waves can suppress the build-up of an intracavity probe field. Mathematically, these processes are captured by the Langevin equations of motion for the complex ampli-

tudes A^- and X, which require in the steady state

$$(-i\Delta' + \kappa/2)\, A^- = -ig_0\bar{a}X + \sqrt{\eta_{\mathrm{c}}\kappa}\,\delta s_{\mathrm{in}} \quad (3)$$

$$2m_{\mathrm{eff}}\Omega_{\mathrm{m}}(-i\Delta' + \Gamma_{\mathrm{m}}/2)\, X = -i\hbar g_0\bar{a}A^-, \quad (4)$$

where we have assumed a high-quality factor of the mechanical oscillator and the control beam detuning $\bar{\Delta} = -\Omega_{\mathrm{m}}$. The amplitude of the probing field launched into the cavity is denoted as δs_{in} and we abbreviate $\Delta' \equiv \Omega - \Omega_{\mathrm{m}}$ (see appendix).

The solution for the probe field

$$A^- = \frac{\sqrt{\eta_{\mathrm{c}}\kappa}}{(-i\Delta' + \kappa/2) + \frac{\Omega_{\mathrm{c}}^2/4}{-i\Delta' + \Gamma_{\mathrm{m}}/2}}\delta s_{\mathrm{in}} \quad (5)$$

is of a form well-known from the response of an EIT medium to a probe field [39]. Indeed, the coherence between the two ground states of an atomic Λ system, and the coherence between the levels probed by the probe laser undergo the very same evolution as do the mechanical oscillation amplitude and the intracavity probe field in the case of OMIT. The role of the control laser's Rabi frequency in an atomic system is taken by the optomechanical coupling rate $\Omega_{\mathrm{c}} = 2\bar{a}g_0 x_{\mathrm{zpf}}$, where $x_{\mathrm{zpf}} = \sqrt{\hbar/2m_{\mathrm{eff}}\Omega_{\mathrm{m}}}$ designates the zero point spread of the mechanical oscillator. For $\Omega_{\mathrm{c}} > \Gamma_{\mathrm{m}}, \kappa$, the system enters the strong coupling regime [11, 40] investigated recently in the mechanical domain [16], in which the optical and mechanical systems are hybridized to dressed states which differ by $\hbar\Omega_{\mathrm{c}}$ in their energy. Only the static radiation pressure bistability sets an upper limit for the coupling rate, in the resolved sideband regime $(\bar{\Delta} = -\Omega_{\mathrm{m}} \gg \kappa)$ it necessitates $\Omega_{\mathrm{c}} < \Omega_{\mathrm{m}}$ [11, 40].

To realize optomechanically induced transparency we employ toroidal whispering-gallery-mode microresonators shown in figure 2 as optomechanical system of choice [8, 32]. These resonators feature a unique combination of low effective mass m_{eff} and large coupling g_0, and can be engineered to display very low mechanical dissipation Γ_{m} by decoupling the mechanical radial-breathing mode (RBM) from other mechanical modes [15]. The combination of high mechanical frequency Ω_{m} and low optical dissipation κ furthermore allows reaching the resolved-sideband regime [41] as discussed above. The parameters of the device used in the experiments presented here are given by $(m_{\mathrm{eff}}, g_0/2\pi, \Gamma_{\mathrm{m}}/2\pi, \Omega_{\mathrm{m}}/2\pi, \kappa/2\pi) \approx (20\,\mathrm{ng}, -12\,\mathrm{GHz/nm}, 41\,\mathrm{kHz}, 51.8\,\mathrm{MHz}, 15\,\mathrm{MHz})$, placed well in the resolved-sideband limit [41]. If the probe laser is scanned through the cavity resonance in the absence of the control laser, typically a simple Lorentzian exctinction dip is observed (cf. figure 2). We operate the cavity in the undercoupled regime, which together with modal coupling between counterpropagating modes (see appendix) leads to a non-zero probe (amplitude) transmission $t_r = t_p(\Delta' = 0, \Omega_{\mathrm{c}} = 0)$ at resonance even in the absence of the control beam. In the case of the present device, $|t_r|^2 \approx 0.5$ (note that $|t_{\mathrm{r}}|^2 < 0.01$ can be achieved

with silica toroids [42]). To separate the effects of this residual transmission from OMIT, we introduce the normalized transmission of the probe $t'_\mathrm{p} = (t_\mathrm{p} - t_\mathrm{r})/(1 - t_\mathrm{r})$.

As shown in figure 2, the experiment was carried out at cryogenic temperatures using a Helium-3 buffer gas cryostat. In addition to reducing the thermal Brownian motion of the mechanical oscillator this allows eliminating thermo-optical nonlinearities [43] which can impede driving the lower motional sideband with a strong control laser. The sample is mounted on a cryogenic head, which allows approaching a tapered fiber for near field evanescent coupling using piezoelectric positioners. While an external-cavity diode laser was used for initial characterization, a low-noise, continuous-wave Titanium Sapphire operating at a wavelength of $\lambda \approx 775\,\mathrm{nm}$ is employed for the actual OMIT experiments. The Ti:sapphire laser's linewidth is reduced below $30\,\mathrm{kHz}$ by stabilization to a temperature-controlled reference cavity using the Pound-Drever-Hall technique. This approach furthermore proved to provide sufficient mutual frequency stability of the cryogenic microresonator and the cavity-stabilized laser on the relevant scale of the cavity linewidth κ.

To detect the mechanical motion at low temperatures we employ a balanced homodyne detection scheme measuring the phase quadrature of the field emerging from the cavity [44]. This allows extracting the resonance frequency $\Omega_\mathrm{m}/2\pi$, quality factor Q_m and effective mass m_eff of the mechanical modes of interest. As in our previous work, we focus on the radial breathing mode of the resonator. The mechanical modes' properties at low temperatures have been detailed in prior work. They feature a complex temperature-dependence of the mechanical resonance frequencies and damping, which agrees excellently with a theoretical model taking into account that mechanical modes can couple to a bath of mechanical two level systems (TLS) via their strain field [43]. For the present toroid micro-resonators thermalized to temperatures in the range of $0.8\,\mathrm{K}$ ($4\,\mathrm{K}$) this results in expected mechanical Q-factor of approximately $Q_\mathrm{m} \approx 10000$ ($Q_\mathrm{m} \approx 1500$). The measured value of $Q_\mathrm{m} = 51.8\,\mathrm{MHz}/41\,\mathrm{kHz} \approx 1300$ at the operating temperature of $3.78\,\mathrm{K}$ agrees well with this prediction.

To probe the cavity absorption spectrum in the presence of a control beam, we induce a frequency-tunable modulation sideband on the Ti:sapphire control laser. We found that the most efficient way to create a sideband tunable over a wide radio-frequency span ($\gg 50\,\mathrm{MHz}$) consists in using a broadband phase modulator driven at the modulation frequency Ω. The laser light sent to the experiment thus consists of the carrier (which is used as control field at a frequency ω_l), the probe beam at the frequency $\omega_\mathrm{p} = \omega_\mathrm{l} + \Omega$, and an additional field at $\omega_\mathrm{l} - \Omega$. Keeping the laser detuned to the lower motional sideband of the cavity ($\bar{\Delta} \approx -\Omega_\mathrm{m}$), a sweep of the modulation frequency Ω scans the probe field through the cavity resonance. In the RSB regime, the *lower* laser sideband induced by phase modulation (at the frequency $\omega_\mathrm{l} - \Omega$) is far detuned (by $|\bar{\Delta} - \Omega| \gg \kappa$) from the cavity resonance in this situation and does not significantly interact with the optomechanical system. It does however play a role in the homodyne detection scheme used. As shown in detail in the appendix, demodulation of the total homodyne signal at the modulation frequency Ω using a network analyzer (NA) allows extracting a 'transmission' homodyne signal t_hom, which, in the RSB regime, is related to the probe transmission by the simple relation $t_\mathrm{hom} \approx 1 - t_\mathrm{p}$.

Figure 3a) shows the theoretically expected response of the optomechanical system and the detected signals due to the combined presence of a control field (tuned to $\bar{\Delta} = -\Omega_\mathrm{m}$) and a frequency-swept probing field. Clearly, the OMIT dip is apparent in the intracavity probe power as described by equation (5). It occurs simultaneously with the onset of radiation-pressure-driven mechanical oscillations, as expected from our model. The excitation of the intracavity probe field therefore is suppressed, and the transmitted field nearly equals the probe field sent to the cavity. The lowest panel shows the homodyne signal expected in such a situation, and the five panels in 3b) show experimentally measured homodyne traces for the detunings $\bar{\Delta}/2\pi \in \{-69.1\,\mathrm{MHz}, -57.6\,\mathrm{MHz}, -51.8\,\mathrm{MHz}, -44.6\,\mathrm{MHz}, -35.4\,\mathrm{MHz}\}$, and a control laser power of $0.5\,\mathrm{mW}$. For different detunings of the control field $\bar{\Delta}$, the center of the probe response to the optical cavity occurs for the modulation frequencies $\Omega \approx -\bar{\Delta}$, since the probe laser then matches the cavity resonance ($\omega_\mathrm{p} \approx \omega_\mathrm{c}$). Importantly however, the sharp OMIT window occurs only when the two-photon resonance condition $\Omega = \Omega_\mathrm{m}$ (with $\Omega = \omega_\mathrm{p} - \omega_\mathrm{l}$) is met, independent of the detuning $\bar{\Delta}$ of the control beam—giving clear evidence to the theoretically suggested underlying mechanism.

To analyze the effect of the control beam more systematically, its detuning was fixed to the lower motional sideband. Varying its power from 0.125 to $6.5\,\mathrm{mW}$, traces of the homodyne signal are taken in the vicinity of the two-photon resonance (figure 4). Dips of increasing depth and width are observed, which can be modeled by a simple Lorentzian function. The minimum homodyne signal is obtained under the condition of the two-photon resonance $\Delta' = 0$. In this case, the homodyne signal power and the probe power transmission are simply interrelated by $|t'_\mathrm{p}|^2 = (1 - |t'_\mathrm{hom}|)^2$, where $t'_\mathrm{hom} = t_\mathrm{hom}/(1 - t_\mathrm{r})$ is the normalized homodyne signal. From the model (5), the expected probe transmission on resonance is simply given by

$$t'_\mathrm{p}(\Delta' = 0) = \frac{C}{C + 1}, \qquad (6)$$

where $C \equiv \Omega_\mathrm{c}^2/\Gamma_\mathrm{m}\kappa$ is an equivalent optomechanical cooperativity parameter. Our data match the expected curve very well if we allow for a linear correction factor in the optomechanical coupling frequency Ω_c due to modal coupling and taper losses in the cryostat (see appendix).

We have reached probe power transmission $|t'_\mathrm{p}|^2$ up to 81%, indicating the high contrast which can be achieved in OMIT. Higher values of C could already be achieved by cooling the device to a lower temperature.

The simple relation between the homodyne signal and the probe transmission furthermore implies that the width Γ_OMIT of the coupling-induced transmission window in $|t'_p|^2$ equals the width of the measured dip in the normalized homodyne signal $|t'_\mathrm{hom}|^2$. The values extracted from our data are shown in figure 4c along with the expected behaviour

$$\Gamma_\mathrm{OMIT} \approx \Gamma_\mathrm{m}(1 + C), \qquad (7)$$

with transparency windows wider than $500\,\mathrm{kHz}$ achieved in our experiment.

Concerning the implications of this work, we note that in any optomechanical system reaching a cooperativity parameter C of order unity, the probe transmission can be significantly altered by the control beam, as desired, for example, in all-optical switches. Interestingly, the systems available already today, reach $C \approx 1$ with only thousands [21] or even hundreds [18, 41] of control photons in the cavity, and recently emerging integrated nano-optomechanical structures [19] may be able to further reduce this number. The resulting extreme optical non-linearities could be of interest for both fundamental and applied studies.

The tunable probe transmission window by necessity also modifies the propagation dynamics of a probe pulse sent to the optomechanical system due to the variation of the complex phase picked by its different frequency components. Indeed, a probe pulse centered at the (shifted) cavity resonance frequency $\omega_\mathrm{c} + g_0\bar{x}$ experiences a group delay of $\tau_\mathrm{g} \approx 2/\Gamma_\mathrm{OMIT}$ in the regime $C \gtrsim 1$ of interest (see appendix). Group delays up to Γ_m^{-1} can therefore be achieved, exceeding times of several seconds in some available optomechanical systems [17]. However, undistorted pulse propagation only occurs if the full probe pulse spectrum is contained within the transparency window of the system. This restricts the effectivity of such a delay due to the fixed delay-bandwidth product of $\tau_\mathrm{g}\Gamma_\mathrm{OMIT} \approx 2$. A cascade of systems may alleviate this shortcoming—the most interesting scenario being a large array of concatenated optomechanical systems. The group delay could then be dynamically tuned while the probe pulse is propagating through the array [7, 8, 13]. Such systems are closely related to an array of coupled *optical* resonators, for which the possibility of light storage has been derived previously [45], and could be practically implemented in lithographically designed optomechanical systems both in the microwave [18] and optical [20] domain.

Author contributions AS contributed the theoretical idea and suggested the measurements. RR, SW and SD constructed the cryogenic setup and performed the measurements. EG fabricated the employed samples. OA contributed at an early stage of the experiment. AS, SW, SD and TJK analyzed the data and wrote the manuscript.

[1] M. Fleischhauer, A. Imamoglu, and J. P. Marangos. Electromagnetically induced transparency: Optics in coherent media. *Review of Modern Physics*, 77:633–673, 2005.

[2] S. E. Harris. Electromagnetically induced transparency. *Physics Today*, 50:36–42, 1997.

[3] A. Kasapi, M. Jain, G. E. Yin, and S. E. Harris. Electromagnetically induced transparency: Propagation dynamics. *Physical Review Letters*, 74(13):2447–2450, Mar 1995.

[4] L. V. Hau, S. E. Harris, Z. Dutton, and C. H. Behroozi. Light speed reduction to 17 metres per second in an ultracold atomic gas. *Nature*, 397:594–598, 1999.

[5] D. F. Phillips, A. Fleischhauer, A. Mair, R. L. Walsworth, and M. D. Lukin. Storage of light in atomic vapor. *Physical Review Letters*, 86:783–786, 2001.

[6] C. Liu, Z. Dutton, C.H. Behroozi, and L.V. Hau. Observation of coherent optical information storage in an atomic medium using halted light pulses. *Nature*, 409:490–493, 2001.

[7] A. Schliesser. *Cavity Optomechanics and Optical Frequency Comb Generation with Silica Whispering-Gallery-Mode Microresonators*. PhD thesis, Ludwig-Maximilians-Universität München, 2009. http://edoc.ub.uni-muenchen.de/10940/, page 121ff.

[8] A. Schliesser and T. J. Kippenberg. Cavity optomechanics with silica microresonators. In E. Arimondo, P. Berman, and C. C. Lin, editors, *Advances in atomic, molecular and optical physics*, volume 58. Elsevier Academic Press, 2010. (in print, preprint at arXiv:1003.5922).

[9] G. S. Agarwal and S. Huang. Electromagnetically induced transparency in mechanical effects of light. *Physical Review A*, 81:041803, 2010.

[10] J. Zhang, K. Peng, and S. L. Braunstein. Quantum-state transfer from light to macroscopic oscillators. *Physical Review A*, 68:013808, 2003.

[11] F. Marquardt, J. P. Chen, A. A. Clerk, and S. M. Girvin. Quantum theory of cavity-assisted sideband

cooling of mechanical motion. *Physical Review Letters*, 99:093902, 2007.

[12] I. Wilson-Rae, N. Nooshi, W. Zwerger, and T. J. Kippenberg. Theory of ground state cooling of a mechanical oscillator using dynamical backaction. *Physical Review Letters*, 99(9):093901, 2007.

[13] D. E. Chang, A. H. Safavi-Naeini, M. Hafezi, and O. Painter. Slowing and stopping light using an optomechanical crystal array. *arXiv:1006.3829*, 2010.

[14] O. Arcizet, P.-F. Cohadon, T. Briant, M. Pinard, and A. Heidmann. Radiation-pressure cooling and optomechanical instability of a micromirror. *Nature*, 444:71–74, 2006.

[15] G. Anetsberger, R. Rivière, A. Schliesser, O. Arcizet, and T. J. Kippenberg. Ultralow-dissipation optomechanical resonators on a chip. *Nature Photonics*, 2:627–633, 2008.

[16] S. Gröblacher, K. Hammerer, M. R. Vanner, and M. Aspelmeyer. Observation of strong coupling between a micromechanical resonator and an optical cavity field. *Nature*, 460:724–727, 2009.

[17] J. D. Thomson, B. M. Zwickl, A. M. Jayich, F. Marquardt, S. M. Girvin, and J. G. E. Harris. Strong dispersive coupling of a high finesse cavity to a micromechanical membrane. *Nature*, 452:72–75, 2008.

[18] C. A. Regal, J. D. Teufel, and K. W. Lehnert. Measuring nanomechanical motion with a microwave cavity interferometer. *Nature Physics*, 4:555–560, 2008.

[19] M. Eichenfield, R. Camacho, J. Chan, K. Vahala, and O. Painter. A picogram and nanometer scale photonic crystal opto-mechanical cavity. *Nature*, 459:550–555, 2009.

[20] M. Eichenfield, J. Chan, R. M. Camacho, K. J. Vahala, and O. Painter. Optomechanical crystals. *Nature*, 462:78–82, 2009.

[21] G. Anetsberger, O. Arcizet, Q. P. Unterreithmeier, R. Rivière, A. Schliesser, E. M. Weig, J. P. Kotthaus, and T. J. Kippenberg. Near-field cavity optomechanics with nanomechanical oscillators. *Nature Physics*, 5:909–914, 2009.

[22] T. J. Kippenberg and K. J. Vahala. Cavity Optomechanics: Back-Action at the Mesoscale. *Science*, 321:1172–1176, 2008.

[23] K.-J. Boller, A. Imamoğlu, and S. E. Harris. Observation of electromagnetically induced transparency. *Physical Review Letters*, 66(20):2593–2596, May 1991.

[24] M. D. Lukin and A. Imamoğlu. Controlling photons using electromagnetically induced transparency. *Nature*, 413(6853):273–276, Sep 2001.

[25] A. V. Turukhin, V. S. Sudarshanam, M. S. Shahriar, J. A. Musser, B. S. Ham, and P. R. Hemmer. Observation of ultraslow and stored light pulses in a solid. *Physical Review Letters*, 88(2):023602, Jan 2002.

[26] P. R. Hemmer, A. V. Turukhin, M. S. Shahriar, and J. A. Musser. Raman-excited spin coherences in nitrogen-vacancy color centers in diamond. *Opt Lett*, 26(6):361–363, Mar 2001.

[27] Daniel Brunner, Brian D Gerardot, Paul A Dalgarno, Gunter Wst, Khaled Karrai, Nick G Stoltz, Pierre M Petroff, and Richard J Warburton. A coherent single-hole spin in a semiconductor. *Science*, 325(5936):70–72, Jul 2009.

[28] N. Liu, L. Langguth, Th. Weiss, J. Kästel, M. Fleischhauer, T. Pfau, and H. Giessen. Plasmonic analogue of electromagnetically induced transparency at the drude damping limit. *Nature Materials*, 8(9):758–762, Sep 2009.

[29] Q. Xu, S. Sandhu, M. L. Povinelli, J. Shakya, S. Fan, and M. Lipson. Experimental realization of an on-chip all-optical analogue to electromagnetically induced transparency. *Physical Review Letters*, 96(12):123901, Mar 2006.

[30] K. Totsuka, N. Kobayashi, and M. Tomita. Slow light in coupled-resonator-induced transparency. *Physical Review Letters*, 98(21):213904, May 2007.

[31] D. D. Smith, H. Chang, K. A. Fuller, A. T. Rosenberger, and R. W. Boyd. Coupled-resonator-induced transparency. 69:063804, 2004.

[32] T. J. Kippenberg, H. Rokhsari, T. Carmon, A. Scherer, and K. J. Vahala. Analysis of Radiation-Pressure Induced Mechanical Oscillation of an Optical Microcavity. *Physical Review Letters*, 95:033901, 2005.

[33] A. Schliesser, P. Del'Haye, N. Nooshi, K.J. Vahala, and T. Kippenberg. Radiation pressure cooling of a micromechanical oscillator using dynamical backaction. *Physical Review Letters*, 97:243905, 2006.

[34] S. Gigan, H. R. Böhm, M. Paternosto, F. Blaser, G. Langer, J. B. Hertzberg, K. C. Schwab, D. Bäuerle, M. Aspelmeyer, and A. Zeilinger. Self-cooling of a micromirror by radiation pressure. *Nature*, 444:67–70, 2006.

[35] Q. Lin, J. Rosenberg, D. Chang, R. Camacho, M. Eichenfield, K. J. Vahala, and O. Painter. Coherent mixing of mechanical excitations in nano-optomechanical structures. *Nature Photonics*, 4:236–242, 2010.

[36] E. Mücke, M. nd Figueroa, J. Bochmann, C. Hahn, K. Murr, S. Ritter, C. J. Villas-Boas, and G. Rempe. Electromagnetically induced transparency with single atoms in a cavity. *Nature*, 465:755–758, 2010.

[37] C. Fabre, M. Pinard, S. Bourzeix, A. Heidmann, E. Giacobino, and S. Reynaud. Quantum-noise reduction using a cavity with a movable mirror. *Physical Review A*, 49:1337–1343, 1994.

[38] S. Mancini and P. Tombesi. Quantum noise reduction by radiation pressure. *Physical Review A*, 49:4055–4065, 1994.

[39] P. W. Milonni. *Fast light, slow light and left-handed light.* Taylor and Francis, 2005.

[40] J. M. Dobrindt, I. Wilson-Rae, and T. J. Kippenberg. Parametric normal-mode splitting in cavity optomechanics. *Physical Review Letters*, 101:263602, 2008.

[41] A. Schliesser, R. Rivière, G. Anetsberger, O. Arcizet, and T. Kippenberg. Resolved-sideband cooling of a micromechanical oscillator. *Nature Physics*, 4:415–419, 2008.

[42] M. Cai, O. Painter, and K. J. Vahala. Observation of critical coupling in a fiber taper to a silica-microsphere whispering-gallery mode system. *Physical Review Letters*, 85(1):74–77, 2000.

[43] O. Arcizet, R. Rivière, A. Schliesser, G. Anetsberger, and T. J. Kippenberg. Cryogenic properties of op- tomechanical silica microcavities. *Physical Review A*, 80:021803(R), 2009.

[44] A. Schliesser, O. Arcizet, R. Rivière, G. Anetsberger, and T. Kippenberg. Resolved-sideband cooling and position measurement of a micromechanical oscilla- tor close to the Heisenberg uncertainty limit. *Nature Physics*, 5:509–514, 2009.

[45] M. F. Yanik and S. Fan. Stopping light all optically. *Physical Review Letters*, 92(8):083901, Feb 2004.
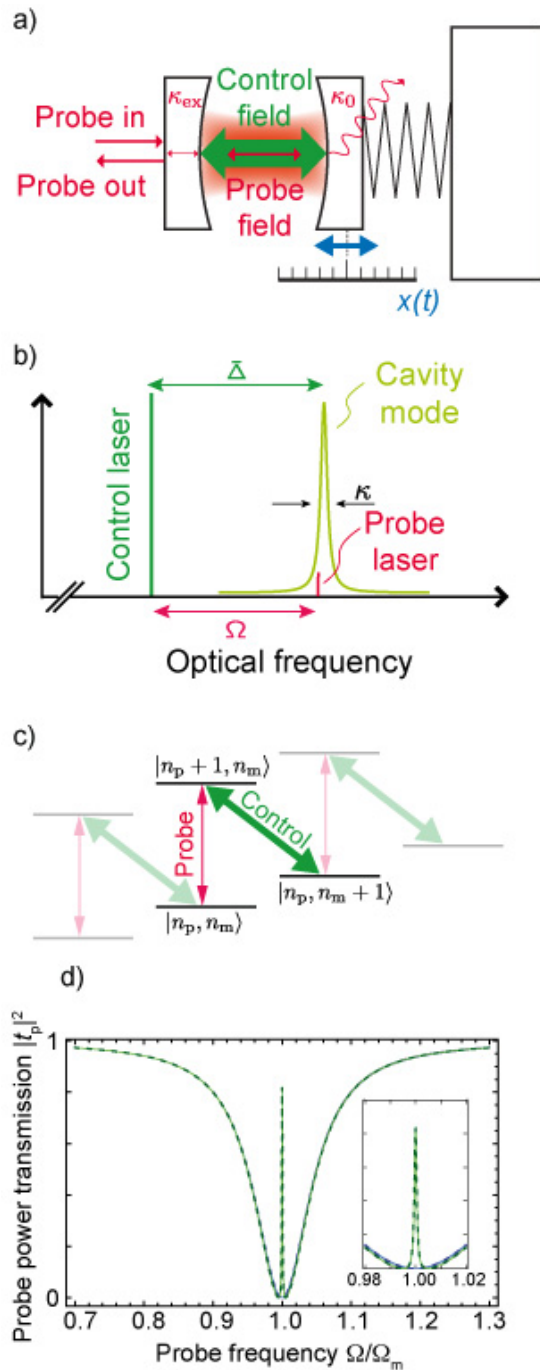
FIG. 1: Optomechanically induced transparency. (a) A generic optomechanical system consists of an optical cavity with a movable boundary, illustrated here as a Fabry-Perot-type resonator in which one mirror acts like a mass-on-a-spring movable along x. The cavity has an intrinsic photon loss rate κ_0 and is coupled to an external propagating mode at the rate κ_{ex}. Through the external mode, the resonator is populated with a control field (only intracavity field is shown). The response of this driven optomechanical system is probed by a weak probe field sent towards the cavity, the transmission of which (i.e. the returned field "Probe out") is analyzed here. (b) The frequency of the control field is detuned by $\bar{\Delta}$ from the cavity resonance frequency, where a detuning close to the lower mechanical sideband, $\bar{\Delta} \approx -\Omega_{\mathrm{m}}$, is chosen. The probe laser's frequency is offset by the tunable radio frequency Ω from the control laser. The dynamics of interest occur when the probe laser is tuned over the optical resonance of the cavity, which has a linewidth of $\kappa = \kappa_0 + \kappa_{\mathrm{ex}}$. (c) Level scheme of the optomechanical system. The control field is tuned close to red-sideband transitions, in which a mechanical excitation quantum is annihilated (mechanical occupation $n_{\mathrm{m}} \to n_{\mathrm{m}} - 1$) when a photon is added to the cavity (optical occupation $n_{\mathrm{p}} \to n_{\mathrm{p}} + 1$), therefore coupling the corresponding energy eigenstates. The probe field probes transitions in which the mechanical oscillator occupation is unchanged. (d) Transmission of the probe laser power through the optomechanical system in the case of a critically coupled cavity $\kappa_0 = \kappa_{\mathrm{ex}}$ as a function of normalized probe frequency offset, when the control field is off (blue lines) and on (green lines). Dashed and full lines correspond to the models based on the full (eq. (1)) and approximative (eq. (5)) calculations, respectively.
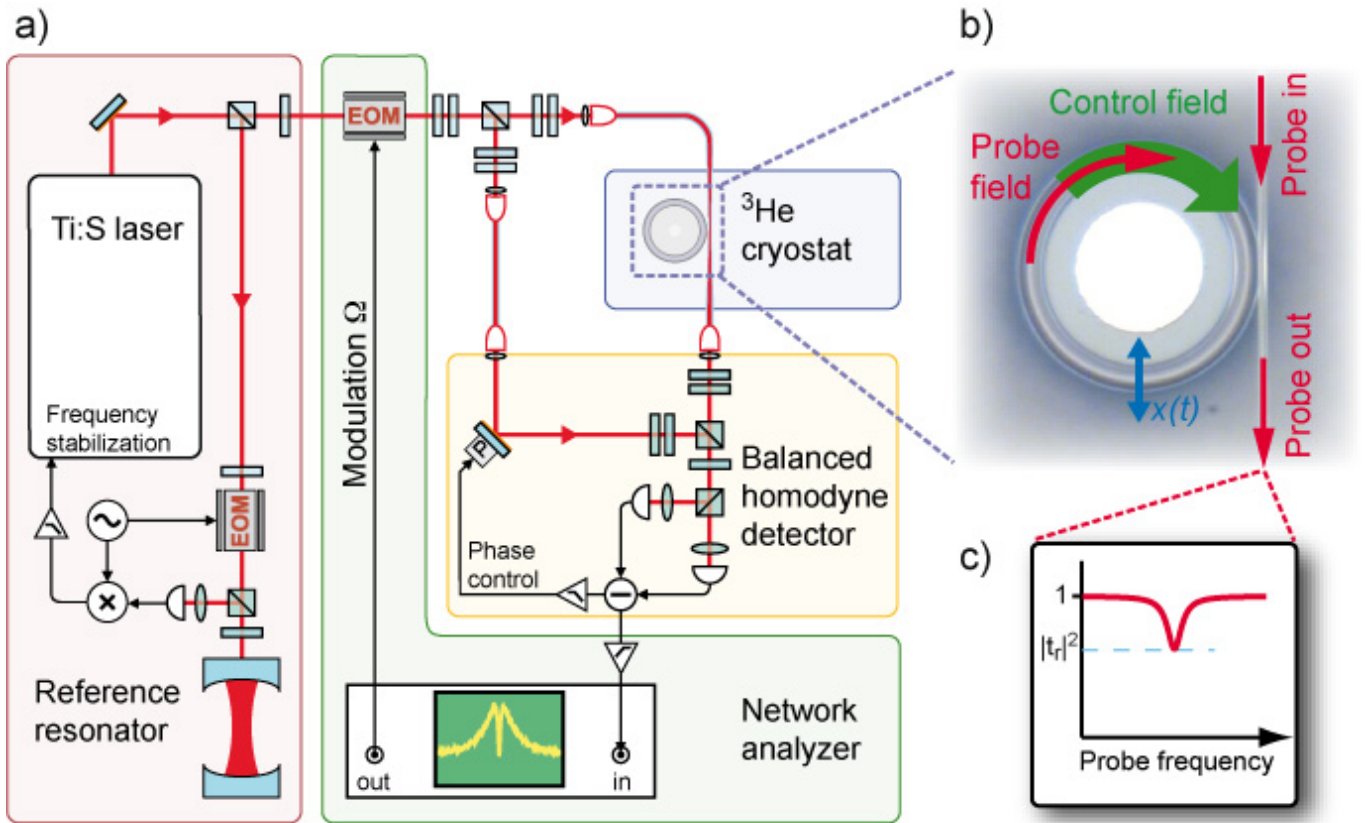
FIG. 2: Experimental setup. a) An optomechanical system consisting of a toroid microresonator held at cryogenic temperatures in a Helium-3 buffer gas cryostat. The control and probe fields are derived from a single Ti:sapphire laser, which is stabilized to an external reference resonator using the Pound-Drever-Hall technique. While the laser carrier is used as control beam, the probe beam is created by a phase modulator driven at the radio frequency Ω. This optical input is split into two arms, one of which is sent to a tapered fiber in the cryostat, which allows optical coupling to the whispering gallery mode of the toroidal resonator as shown in micrograph with a $\sim 60\,\mu$m-diameter toroid. The other arm serves as the local oscillator in a balanced homodyne receiver used to analyze the light returned from the optomechanical system. While the receiver's DC component is used to lock the phase of the local oscillator, the AC component is analyzed using a network analyzer. c) In absence of the control beam, the transmission of the probe is a simple Lorentzian. Under the chosen waveguid-toroid coupling conditions, there is a non-zero probe power transmission $|t_{\mathrm{r}}|^2$ at resonance.
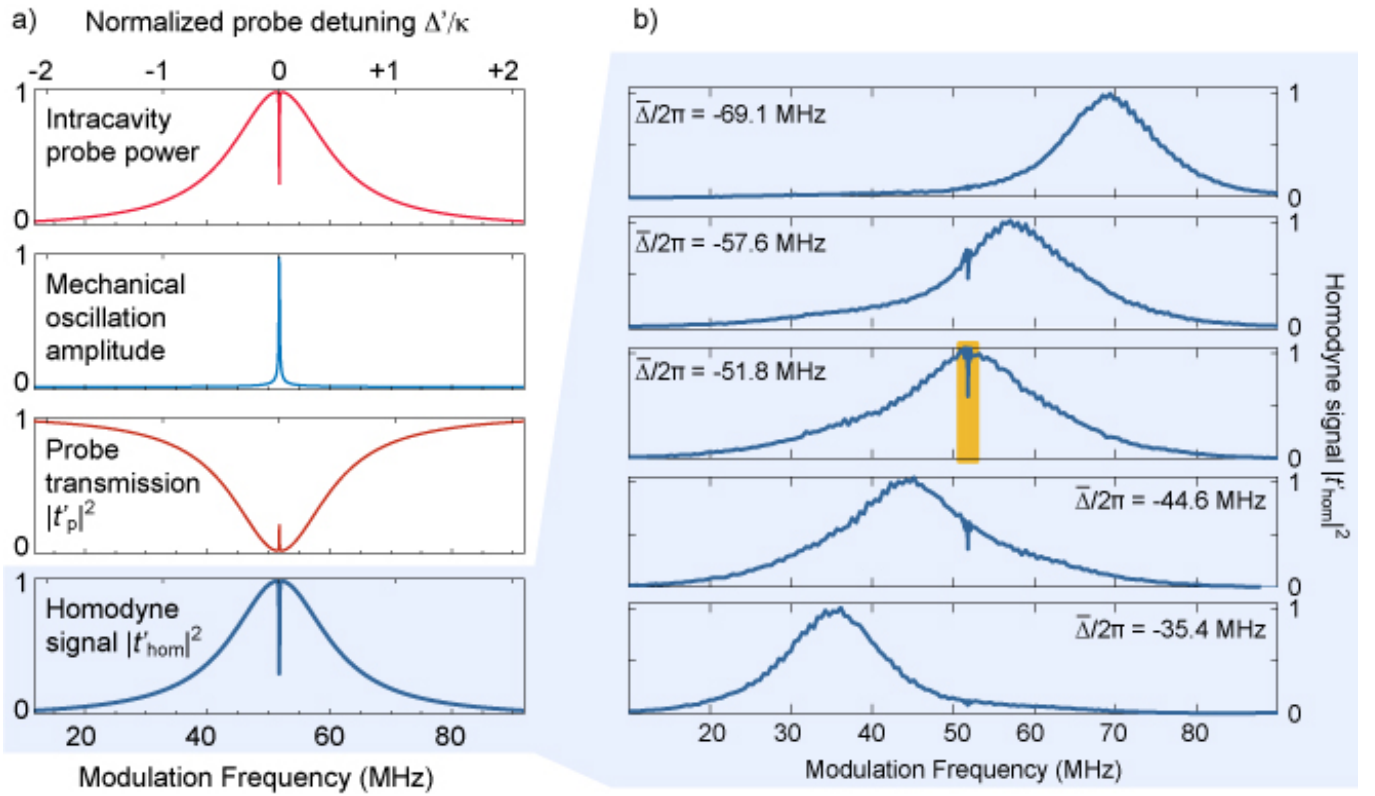
FIG. 3: Observation of OMIT. a) Theoretically expected intracavity probe power $|A^-|^2$, oscillation amplitude X, probe power transmission $|t_\mathrm{p}|^2$ and the homodyne signal $|t_\mathrm{hom}|^2$ as a function of the modulation frequency $\Omega/2\pi$ (top to bottom panels). The first two panels have additionally been normalized to unity. When the two-photon resonance condition is met, the mechanical oscillator is excited $\Delta' = 0$, giving rise to destructive interference of excitation pathways for an intracavity probe field. The probe transmission therefore exhibits an inverted dip, which can be easily identified in the homodyne signal. b) Experimentally observed normalized homodyne traces when the probe frequency is scanned by sweeping the phase modulator frequency Ω for different values of control beam detuning $\bar{\Delta}$. While the center of the response of the bare optical cavity shifts correspondingly, the sharp dip characteristic of OMIT occurs always for $\Delta' = 0$. The power of the control beam sent to the cavity is 0.5 mW in these measurements and the He-3 buffer gas has a pressure of 155 mbar at a temperature of 3.8 K. The middle panel shows the operating conditions where the control beam is tuned to the lower motional sideband $\bar{\Delta} \approx -\Omega_\mathrm{m} = -2\pi \cdot 51.8$ MHz. The region around the central dip (orange background) is studied in more detail in a dedicated experimental series (cf. figure 4).
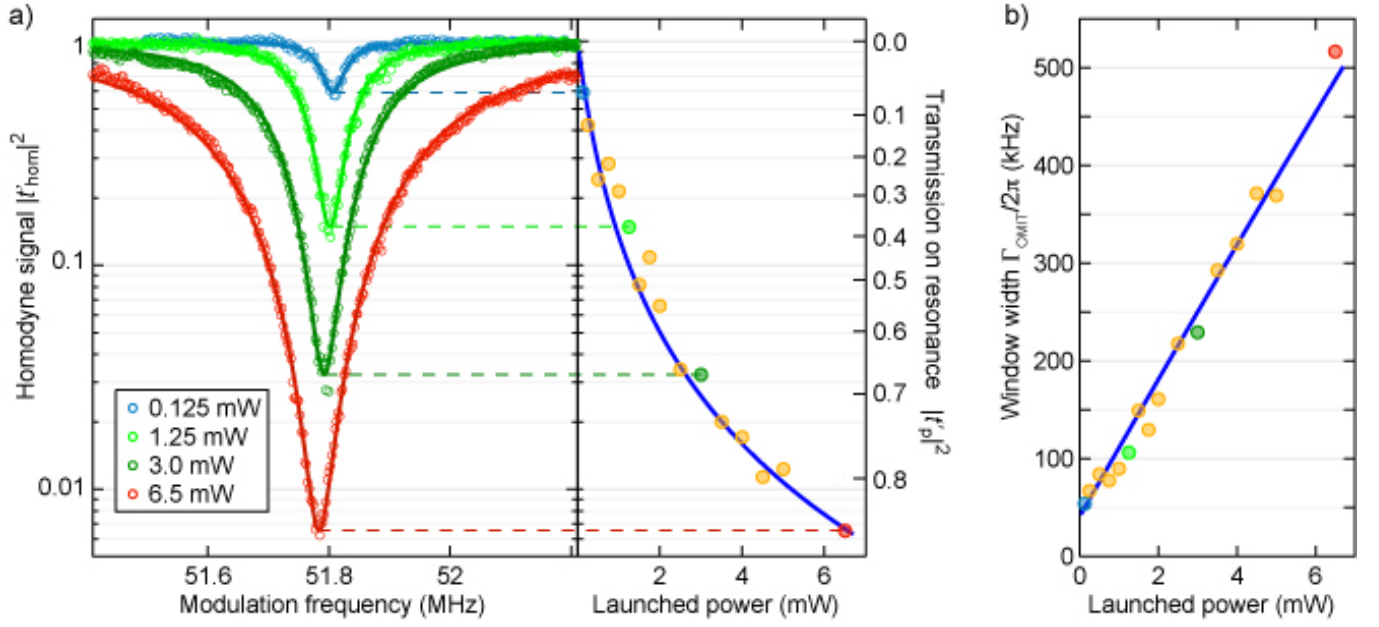
FIG. 4: Controlling optomechanically induced transparency. a) Experimental normalized homodyne traces in the presence of a control beam (circles) for four different powers in the control beam from $0.125\,\text{mW}$ up to $6.5\,\text{mW}$, and Lorentzian models. The minimum homodyne signal (measured at $\Delta' = 0$) directly indicates the maximum probe power transmission achieved in this case. These values are given in the right panel for a larger set of probe scans, together with the theoretical model developed in this work. See text for more information. b) Width of the transparency window extracted from the same set of probe scans. Good agreement with the theoretical prediction is found over the entire power range.

Appendix - Optomechanically induced transparency

S 1. DERIVATION OF OMIT

In the following, we derive the expressions describing the optomechanical equivalent of Electromagnetically Induced Transparency (EIT), as discussed in [1, 2], as well as more recent analysis [3]. The starting point of the following analysis is the Hamiltonian formulation of a generic optomechanical system put forward by Law [4].

A. Hamiltonian

If the free spectral range of the cavity is much larger than the mechanical oscillation frequency, such that only one optical mode is coupled to the mechanical mode, the optomechanical Hamiltonian can be written as:

$$\hat{H} = \hat{H}_{\text{mech}} + \hat{H}_{\text{opt}} + \hat{H}_{\text{int}} + \hat{H}_{\text{drive}} \tag{S1}$$

$$\hat{H}_{\text{mech}} = \frac{\hat{p}^2}{2m_{\text{eff}}} + \frac{1}{2} m_{\text{eff}} \Omega_{\text{m}}^2 \hat{x}^2 \tag{S2}$$

$$\hat{H}_{\text{opt}} = \hbar \omega_{\text{c}} \left(\hat{a}^\dagger \hat{a} + \frac{1}{2} \right) \tag{S3}$$

$$\hat{H}_{\text{int}} = \hbar g_0 \hat{x} \, \hat{a}^\dagger \hat{a} \tag{S4}$$

$$\hat{H}_{\text{drive}} = i\hbar \, \sqrt{\eta_{\text{c}}\kappa} \left(s_{\text{in}}(t)\hat{a}^\dagger - s_{\text{in}}^*(t)\hat{a} \right), \tag{S5}$$

where $\hat{x}$ and $\hat{p}$ are the position and momentum operators of the mechanical degree of freedom having effective mass m_{eff} and angular frequency Ω_m, and $s_{\text{in}}(t)$ is the drive amplitude normalized to a photon flux at the input of the cavity. $\hat{a}$ and $\hat{a}^\dagger$ are the annihilation and creation operators of the cavity mode. We have furthermore used the coupling parameter $\eta_{\text{c}} \equiv \kappa_{\text{ex}}/\kappa_0 + \kappa_{\text{ex}}$, where κ_0 denotes the intrinsec loss rate and κ_{ex} the external loss rate (i.e. wave guide coupling). Experimentally, the parameter η_{c} can be continuously adjusted by tuning the taper-resonator gap [5, 6].

We will solve this problem for a driving field $s_{\text{in}}(t) = (\bar{s}_{\text{in}} + \delta s_{\text{in}}(t)) \, e^{-i\omega_{\text{l}}t}$, where ω_{l} is the driving laser frequency, and we deliberately identify $\bar{s}_{\text{in}} = s_{\text{l}}$. We will then first derive the linearized Langevin equations [7] for a generic perturbation term $\delta s_{\text{in}}(t)$ before identifying it with the probe field $\delta s_{\text{in}}(t) = s_{\text{p}}e^{-i(\omega_{\text{p}}-\omega_{\text{l}})t}$.

B. Langevin equations

In a frame rotating at ω_{l} with $\Delta = \omega_{\text{l}} - \omega_{\text{c}}$, neglecting quantum and thermal noise we obtain:

$$\frac{d}{dt}\hat{a}(t) = \left(+i\Delta - \frac{\kappa}{2} \right) \hat{a}(t) - ig_0\hat{x}(t)\hat{a}(t) + \sqrt{\eta_{\text{c}}\kappa}s_{\text{in}}(t) \tag{S6}$$

$$\frac{d}{dt}\hat{x}(t) = \frac{\hat{p}(t)}{m_{\text{eff}}} \tag{S7}$$

$$\frac{d}{dt}\hat{p}(t) = -m_{\text{eff}}\Omega_{\text{m}}^2\hat{x}(t) - \hbar g_0\hat{a}^\dagger(t)\hat{a}(t) - \Gamma_{\text{m}}\hat{p}(t), \tag{S8}$$

where the decay rates for the optical (κ) and mechanical oscillators (Γ_m) have been introduced classically. We first denote $\bar{a}$ and $\bar{x}$ the intracavity field and mechanical displacement for the static solution, in which all time derivatives vanish and $s_{\text{p}} \to 0$. From (S6)(S8), it follows immediately that $\bar{a}$ and $\bar{x}$ must fulfill the self consistent equations:

$$\bar{a} = \frac{\sqrt{\eta_{\text{c}}\kappa}}{-i(\Delta - g_0\bar{x}) + \kappa/2}\bar{s}_{\text{in}} \tag{S9}$$

$$\bar{x} = \frac{\bar{a}^2}{m_{\text{eff}}\Omega_m^2}, \tag{S10}$$

where we have assumed a to be real and positive. This system can give rise to bistability for sufficiently strong control fields [8][7]. However, for weak and detuned control fields, only one solution exists and $|\bar{a}|^2 \propto \eta_c \bar{s}_{in}^2$. We then linearize the problem for $\delta s_{in} \ll |\bar{s}_{in}|$, plugging the ansatz $\hat{a}(t) = \bar{a} + \delta\hat{a}(t)$ and $\hat{x}(t) = \bar{x} + \delta\hat{x}(t)$ into equations (S6)(S7)(S8) and retain only first order terms in the small quantities $\delta\hat{a}$, $\delta\hat{a}^\dagger$ and $\delta\hat{x}$. We then obtain

$$\frac{d}{dt}\delta\hat{a}(t) = \left(+i\bar{\Delta} - \frac{\kappa}{2}\right)\delta\hat{a}(t) - ig_0\bar{a}\delta\hat{x}(t) + \sqrt{\eta_c\kappa}\delta s_{in}(t) \tag{S11}$$

$$\frac{d^2}{dt^2}\delta\hat{x}(t) + \Gamma_m\frac{d}{dt}\delta\hat{x}(t) + \Omega_m^2\delta\hat{x}(t) = -\frac{\hbar g_0}{m_{eff}}\bar{a}\left(\delta\hat{a}(t) + \delta\hat{a}^\dagger(t)\right), \tag{S12}$$

where we used the Hermitian property $\delta\hat{x}(t) = \delta\hat{x}^\dagger(t)$ in equation (S11), and introduced the corrected detuning $\bar{\Delta} = \Delta - g_0\bar{x}$. Since the drives are weak, but classical coherent fields, we will identify all operators with their expectation values $y(t) \equiv \langle\hat{y}(t)\rangle$.

C. Solution

1. General solution

We now have to solve the equations of the expectation values for the drive (in the rotating frame) $\delta s_{in}(t) = s_p e^{-i(\omega_p - \omega_l)t}$. For a given $\Omega = \omega_p - \omega_l$ we use the ansatz

$$\delta a(t) = A^- e^{-i\Omega t} + A^+ e^{+i\Omega t} \tag{S13}$$

$$\delta a^*(t) = (A^+)^* e^{-i\Omega t} + (A^-)^* e^{+i\Omega t} \tag{S14}$$

$$\delta x(t) = X e^{-i\Omega t} + X^* e^{+i\Omega t}. \tag{S15}$$

If sorted by rotation terms, this yields six equations. However, the probe field's transmission at frequency $\omega_l + \Omega$ only depends on A^-. In this sense, the three equations of interest are:

$$\left(-i(\bar{\Delta} + \Omega) + \kappa/2\right)A^- = -ig_0\bar{a}X + \sqrt{\eta_c\kappa}s_p \tag{S16}$$

$$\left(+i(\bar{\Delta} - \Omega) + \kappa/2\right)(A^+)^* = +ig_0\bar{a}X \tag{S17}$$

$$m_{eff}\left(\Omega_m^2 - \Omega^2 - i\Gamma_m\Omega\right)X = -\hbar g_0\bar{a}\left(A^- + (A^+)^*\right). \tag{S18}$$

The solution of interest is

$$A^- = \frac{1 + if(\Omega)}{-i(\bar{\Delta} + \Omega) + \kappa/2 + 2\bar{\Delta}f(\Omega)}\sqrt{\eta_c\kappa}s_p, \tag{S19}$$

with

$$f(\Omega) = \hbar g_0^2\bar{a}^2 \frac{\chi(\Omega)}{i(\bar{\Delta} - \Omega) + \kappa/2} \tag{S20}$$

and the mechanical susceptibility

$$\chi(\Omega) = \frac{1}{m_{eff}}\frac{1}{\Omega_m^2 - \Omega^2 - i\Omega\Gamma_m}. \tag{S21}$$

2. Spectrum of the transmitted light

Using the input-output relation [9], one obtains:

$$s_{out}(t) = s_{in}(t) - \sqrt{\eta_c\kappa}\, a(t) \tag{S22}$$

$$= (s_c - \sqrt{\eta_c\kappa}\bar{a})e^{-i\omega_c t} + (s_p - \sqrt{\eta_c\kappa}A^-)e^{-i(\omega_c + \Omega)t} - \sqrt{\eta_c\kappa}A^+ e^{-i(\omega_c - \Omega)t}. \tag{S23}$$

The transmission of the probe beam, defined by the ratio of the output and input field amplitudes at the probe frequency is then given by:

$$t_p = 1 - \sqrt{\eta_c \kappa} A^- \tag{S24}$$

$$= 1 - \frac{1 + if(\Omega)}{-i(\bar{\Delta} + \Omega) + \kappa/2 + 2\bar{\Delta}f(\Omega)} \eta_c \kappa. \tag{S25}$$

3. Resolved-sideband limit

In the resolved sideband regime [10] ($\kappa \ll \Omega_m$), the lower sideband, far off-resonance, can be neglected:

$$A^+ \approx 0.$$

In addition, we can linearize the mechanical susceptibility for small values of the parameter $\Delta' = \Omega - \Omega_m$:

$$m_{\mathrm{eff}}(\Omega_m^2 - \Omega^2 - i\Gamma_m\Omega) \approx \Omega_m(2\Delta' - i\Gamma_m).$$

The system (S16)(S17)(S18) then simplifies to:

$$\left(-i(\bar{\Delta} + \Omega_m + \Delta') + \kappa/2\right)A^- = -ig_0\bar{a}X + \sqrt{\eta_c\kappa}s_p \tag{S26}$$

$$\Omega_m(2\Delta' - i\Gamma_m)X = -\hbar g_0\bar{a}A^-. \tag{S27}$$

The solution for the intracavity field is:

$$A^- = \frac{\sqrt{\eta_c\kappa}s_p}{-i(\bar{\Delta} + \Omega_m + \Delta') + \kappa/2 + \frac{\Omega_c^2/4}{(-i\Delta' + \Gamma_m/2)}}, \tag{S28}$$

where we have introduced the coupling between the mechanical and optical resonators:

$$\Omega_c = 2g_0\bar{a}x_{\mathrm{zpf}},$$

with

$$x_{\mathrm{zpf}} = \sqrt{\frac{\hbar}{2m_{\mathrm{eff}}\Omega_m}},$$

the zero point fluctuations amplitude of the mechanical oscillator. This formula becomes

$$A^- = \frac{\sqrt{\eta_c\kappa}s_p}{-i\Delta' + \kappa/2 + \frac{\Omega_c^2/4}{(-i\Delta' + \Gamma_m/2)}} \tag{S29}$$

for a control laser tuned to the lower motional sideband ($\bar{\Delta} = -\Omega_m$). We will now briefly review the formalism used to describe EIT in the context of atomic physics to emphasize the analogy between the two phenomena.

S 2. ATOMIC EIT

For atomic EIT, we essentially revisit the well-known derivation developed in [11], which will assist in identifying the close resemblance between OMIT and atomic EIT. We consider a Λ-system, consisting of a common upper state $|3\rangle$ and two (long-lived) ground states $|1\rangle$ and $|2\rangle$. In a semiclassical treatment [12], the relevant Hamiltonian is given by:

$$\hat{H} = \sum_j \hbar\omega_j\hat{\sigma}_{jj} - \frac{\hbar}{2}\mu_{23}(\hat{\sigma}_{23} + \hat{\sigma}_{32})E(t) - \frac{\hbar}{2}\mu_{13}(\hat{\sigma}_{13} + \hat{\sigma}_{31})E(t), \tag{S30}$$

where $\hat{\sigma}_{ij} = |i\rangle\langle j|$ are the atomic projection operators and $i, j \in \{1, 2, 3\}$ label the three involved levels. ω_{ij} and μ_{ij} are the frequency and dipole moment along the electric field's direction for the $i \to j$ transition. The (classical) field

contains the two (coupling and probe) components

$$E(t) = \frac{1}{2}\mathcal{E}_c \left(e^{-i\omega_c t} + e^{+i\omega_c t}\right) + \frac{1}{2}\mathcal{E}_p \left(e^{-i\omega_p t} + e^{+i\omega_p t}\right), \tag{S31}$$

where ω_c is tuned close to ω_{32} and ω_p close to ω_{31}. The usual Heisenberg equations of motion for the operators $\hat{\sigma}_{ij}$ can then be derived using $i\hbar\frac{d\hat{\sigma}_{ij}}{dt} = [\hat{\sigma}_{ij}, \hat{H}]$. Retaining only near-resonant terms, the equations of motion can be written as

$$\dot{\hat{\sigma}}_{12} = -i\omega_{21}\hat{\sigma}_{12} + \frac{i}{2\hbar}\mu_{23}\mathcal{E}_c\hat{\sigma}_{13}e^{+i\omega_c t} - \frac{i}{2\hbar}\mu_{13}\mathcal{E}_p\hat{\sigma}_{32}e^{-i\omega_p t} \tag{S32}$$

$$\dot{\hat{\sigma}}_{23} = -i\omega_{32}\hat{\sigma}_{23} + \frac{i}{2\hbar}\mu_{23}\mathcal{E}_c(\hat{\sigma}_{22} - \hat{\sigma}_{33})e^{-i\omega_c t} + \frac{i}{2\hbar}\mu_{13}\mathcal{E}_p\hat{\sigma}_{21}e^{-i\omega_p t} \tag{S33}$$

$$\dot{\hat{\sigma}}_{13} = -i\omega_{31}\hat{\sigma}_{13} + \frac{i}{2\hbar}\mu_{23}\mathcal{E}_c\hat{\sigma}_{12}e^{-i\omega_c t} + \frac{i}{2\hbar}\mu_{13}\mathcal{E}_p(\hat{\sigma}_{11} - \hat{\sigma}_{33})e^{-i\omega_p t}. \tag{S34}$$

We emphasize that the rotating wave approximation (neglecting all non-resonant contributions) is analogous to the resolved sideband approximation presented in the context of OMIT. For a sufficiently weak probe field, the expectation values $\sigma_{ij} = \langle\hat{\sigma}_{ij}\rangle$ can further be approximated to obey $\sigma_{11} \approx 1$ and $\sigma_{22} \approx \sigma_{33} \approx \sigma_{23} \approx \sigma_{32} \approx 0$ at all times, while the remaining expectation values obey

$$\dot{\sigma}_{12} = -i(\omega_{21} - i\gamma_{12}/2)\sigma_{12} + \frac{i}{2\hbar}\mu_{23}\mathcal{E}_c\sigma_{13}e^{+i\omega_c t} \tag{S35}$$

$$\dot{\sigma}_{13} = -i(\omega_{31} - i\gamma_{13}/2)\sigma_{13} + \frac{i}{2\hbar}\mu_{23}\mathcal{E}_c\sigma_{12}e^{-i\omega_c t} + \frac{i}{2\hbar}\mu_{13}\mathcal{E}_p e^{-i\omega_p t}, \tag{S36}$$

where damping rates γ_{12} and γ_{13} were introduced classically. Changing to a rotating frame $\sigma_{12} = S_{12}e^{-i\Omega t}$, $\sigma_{13} = S_{13}e^{-i(\omega_c + \Omega)t}$ and $\mathcal{E}_p e^{-i\omega_p t} = \mathcal{E}_p e^{-i(\omega_c + \Omega)t}$ with $\omega_p = \omega_c + \Omega$, we obtain in the steady state

$$(-i(\Omega - \omega_{21}) + \gamma_{12}/2)S_{12} = +\frac{i}{2\hbar}\mu_{23}\mathcal{E}_c S_{13} \tag{S37}$$

$$(-i(\Omega + \omega_c - \omega_{31}) + \gamma_{13}/2)S_{13} = +\frac{i}{2\hbar}\mu_{23}\mathcal{E}_c S_{12} + \frac{i}{2\hbar}\mu_{13}\mathcal{E}_p, \tag{S38}$$

which is solved by

$$S_{13} = \frac{i\mu_{13}\mathcal{E}_p/2\hbar}{-i(\Delta' + \omega_c - \omega_{32}) + \gamma_{13}/2 + \frac{\Omega_c^2/4}{-i\Delta' + \gamma_{12}/2}}, \tag{S39}$$

where we now abbreviate $\Delta' = \Omega - \omega_{21} = \omega_p - \omega_{31}$. We note as an aside that an equivalent calculation can be made for the atomic coherences ρ_{12} and ρ_{13}, yielding essentially the same result [12]. This result simplifies for a control field on resonance ($\omega_c = \omega_{32}$):

$$S_{13} = \frac{i\mu_{13}\mathcal{E}_p/2\hbar}{-i\Delta' + \gamma_{13}/2 + \frac{\Omega_c^2/4}{-i\Delta' + \gamma_{12}/2}}. \tag{S40}$$

The induced dipole moment along the electric field's direction is given by $p = \mu_{13}(\sigma_{13} + \sigma_{31})$ so that the polarizibility α of the medium at the probe frequency in the presence of the coupling beam can be directly given by

$$\alpha = \frac{\mu_{13}S_{13}}{\mathcal{E}_p/2} = \frac{i\mu_{13}^2/\hbar}{(-i\Delta' + \gamma_{13}/2) + \frac{\Omega_c^2/4}{(-i\Delta' + \gamma_{12}/2)}}. \tag{S41}$$

Evidently one can identify a formal correspondence between the physical entities involved in EIT in atomic physics and OMIT in optomechanical systems. Equations (S37)(S38)(S39)(S40) are perfectly equivalent to (S26)(S27)(S28)(S29) by applying the identifications listed in the following table.

TABLE I: Comparison of physical entities relevant for EIT and OMIT.

EIT	OMIT
projection operator σ_{13} (coherence ρ_{13})	intracavity field amplitude A^-
projection operator σ_{12} (coherence ρ_{12})	mechanical displacement amplitude X
energy difference between ground states $\hbar\omega_{21}$	phonon energy $\hbar\Omega_{\mathrm{m}}$
Rabi frequency $\mu_{23}\mathcal{E}_{\mathrm{c}}/\hbar$	optomechanical coupling rate $2g_0\bar{a}x_{\mathrm{zpf}}$

S 3. SIMPLIFIED EXPRESSIONS IN THE WEAK COUPLING CASE

In addition to the resolved sideband approximation, we will consider the case where the optomechanical coupling is weak compared to the optical losses ($\Omega_c, \Gamma_m \ll \kappa$). We also assume that the control laser is tuned on the lower sideband ($\bar{\Delta} = -\Omega_m$). Then, the EIT feature is very well described by a Lorentzian transmission window in the optical transmission spectrum. This can be seen by applying the simplification $-i\Delta' + \kappa/2 \approx \kappa/2$ in equation (S29):

$$A^- \approx \frac{4\sqrt{\eta_{\mathrm{c}}\kappa}(-i\Delta' + \Gamma_m/2)}{2\kappa(\Gamma_m/2 - i\Delta') + \Omega_c^2} s_p. \tag{S42}$$

Plugging the corresponding value of A^- in (S24), one obtains:

$$t_p = 1 - 2\eta_{\mathrm{c}} + \frac{2\eta_{\mathrm{c}}\Omega_c^2}{\Omega_c^2 + \Gamma_m\kappa - 2i\Delta'\kappa}. \tag{S43}$$

In order to isolate the interesting physics of OMIT from the well-understood waveguide-cavity coupling effects, we introduce the normalized transmission:

$$t_p' = \frac{t_p - t_r}{1 - t_r}, \tag{S44}$$

where t_r is the residual on resonance transmission in the absence of a coupling laser:

$$t_r = t_p(\Delta' = 0, \Omega_c = 0) \tag{S45}$$
$$= 1 - 2\eta_{\mathrm{c}}. \tag{S46}$$

The normalized transmission is then independant of η_{c}:

$$t_p' = \frac{\Omega_c^2}{\Omega_c^2 + \Gamma_m\kappa - 2i\Delta'\kappa}. \tag{S47}$$

This corresponds to the transmission in the case of critical coupling $\eta_{\mathrm{c}} = 1/2$. The optomechanically induced transparency window is hence given by:

$$|t_p'|^2 = \frac{\Omega_c^4/\kappa^2}{(\Omega_c^2/\kappa + \Gamma_m)^2 + (2\Delta')^2}. \tag{S48}$$

A Lorentzian of width

$$\Gamma_{\mathrm{OMIT}} = \Gamma_m + \Omega_c^2/\kappa \tag{S49}$$
$$\tag{S50}$$

and peak value

$$|t_p'(\Delta' = 0)|^2 = \left(\frac{\Omega_c^2/\kappa}{\Gamma_m + \Omega_c^2/\kappa}\right)^2. \tag{S51}$$

These two quantities can be expressed very simply by introducing the cooperativity of the coupled systems $C = \Omega_c^2/(\Gamma_m \kappa)$ [13]:

$$\Gamma_{\text{OMIT}} = \Gamma_m(1 + C) \tag{S52}$$

$$|t'_p(\Delta' = 0)|^2 = \left(\frac{C}{1+C}\right)^2. \tag{S53}$$

S 4. MEASUREMENT USING THE PHASE MODULATION SCHEME

For technical reasons, the optical response was probed using a frequency modulation technique: the coupling laser is phase modulated using an EOM at frequency Ω, hence creating two sidebands at $\omega_l + \Omega$ and $\omega_l - \Omega$. In the resolved sideband regime, only the upper sideband, close to resonance interacts with the cavity, acting as a weak probe beam. The lower one and carrier are transmitted unchanged through the tapered fiber. However, one has to take them into account in order to understand quantitatively the obtained results. We will show here that the measured signal is linked to the transmission at the probe frequency through a direct relation.

The precise measurement scheme is given in figure 2, and reproduced in figure S1. The incident fields at the homodyne beamsplitter are a carrier and two sidebands of the local oscillator, and the carrier and two sidebands of the beam entering the cavity. We note t_c, t_{us} and t_{ls} the complex transmission coefficient across the cavity for the carrier, upper sideband and lower sideband respectively. The phase of the local oscillator Φ is actively adjusted so that it matches the phase of the control beam emerging from the cavity.

At one exit of the beamsplitter the optical power is proportional to

$$\left| E_{\text{cav}} e^{i\omega_l t} \left(t_c + i\frac{\beta}{2} e^{+i\Omega t} t_{\text{us}} + i\frac{\beta}{2} e^{-\Omega t} t_{\text{ls}} \right) + i E_{\text{LO}} e^{i\omega_l t} e^{i\Phi} \left(1 + i\frac{\beta}{2} e^{+i\Omega t} + i\frac{\beta}{2} e^{-i\Omega t} \right) \right|^2, \tag{S54}$$

where β is the depth of the modulation induced by the EOM, E_{LO} and E_{cav} are the field amplitudes in the local oscillator and signal arms of the homodyne setup. The interesting terms are the modulated cross-terms, they are given by

$$
\begin{aligned}
2\,\text{Re}\Bigg[&\left(E_{\text{cav}} e^{i\omega_l t} t_c \right) \cdot \left(i E_{\text{LO}} e^{i\omega_l t} e^{i\Phi} \left(i\frac{\beta}{2} e^{+i\Omega t} + i\frac{\beta}{2} e^{-i\Omega t} \right) \right)^* \\
&+ \left(E_{\text{cav}} e^{i\omega_l t} \left(i\frac{\beta}{2} e^{+i\Omega t} t_{\text{us}} + i\frac{\beta}{2} e^{-i\Omega t} t_{\text{ls}} \right) \right) \cdot \left(i E_{\text{LO}} e^{i\omega_l t} e^{i\Phi} \right)^* \Bigg] \\
= \beta E_{\text{cav}} E_{\text{LO}} \, &\text{Re}\left[t_c \cdot \left(-e^{-i\Phi} \left(e^{-i\Omega t} + e^{+i\Omega t} \right) \right) + \left(e^{+i\Omega t} t_{\text{us}} + e^{-i\Omega t} t_{\text{ls}} \right) \cdot \left(e^{-i\Phi} \right) \right] \\
= \beta E_{\text{cav}} E_{\text{LO}} \, &\text{Re}\left[\left(e^{-i\Phi} \right) \left(-t_c 2\cos(\Omega t) + \left(e^{+i\Omega t} t_{\text{us}} + e^{-i\Omega t} t_{\text{ls}} \right) \right) \right]
\end{aligned}
\tag{S55}
$$

Now writing real and imaginary parts of the used functions as

$$e^{-i\Phi} \equiv \Phi' + i\Phi'' \tag{S56}$$
$$t_c \equiv t'_c + it''_c \tag{S57}$$
$$t_{\text{us}} \equiv t'_{\text{us}} + it''_{\text{us}} \tag{S58}$$
$$t_{\text{ls}} \equiv t'_{\text{ls}} + it''_{\text{ls}} \tag{S59}$$

we get (omitting the prefactor $\beta E_{\text{cav}} E_{\text{LO}}$)

$$\cos(\Omega t) \underbrace{\left(-2\Phi_r t'_c + 2\Phi'' t''_c + (t'_{\text{us}} + t'_{\text{ls}})\Phi' - (t''_{\text{us}} + t''_{\text{ls}})\Phi'' \right)}_{A} + \sin(\Omega t) \underbrace{\left(-(t''_{\text{us}} - t''_{\text{ls}})\Phi' - (t'_{\text{us}} - t'_{\text{ls}})\Phi'' \right)}_{B} \tag{S60}$$

A and B represent the in-phase and quadrature response of the system to the input modulation. In the resolved sideband regime, only the upper sideband is affected by the cavity. In this case $\Phi' = t'_c = t'_{\text{ls}} = 1$ and $\Phi'' = t''_c = t''_{\text{ls}} = 0$. Moreover, the upper sideband, close to resonance, is probing the OMIT signal $t_{\text{us}} = t_p$. The quadratures measured by the network analyzer are then:

$$A \approx 1 - t'_{\text{us}} = 1 - \text{Re}(t_p) \tag{S61}$$
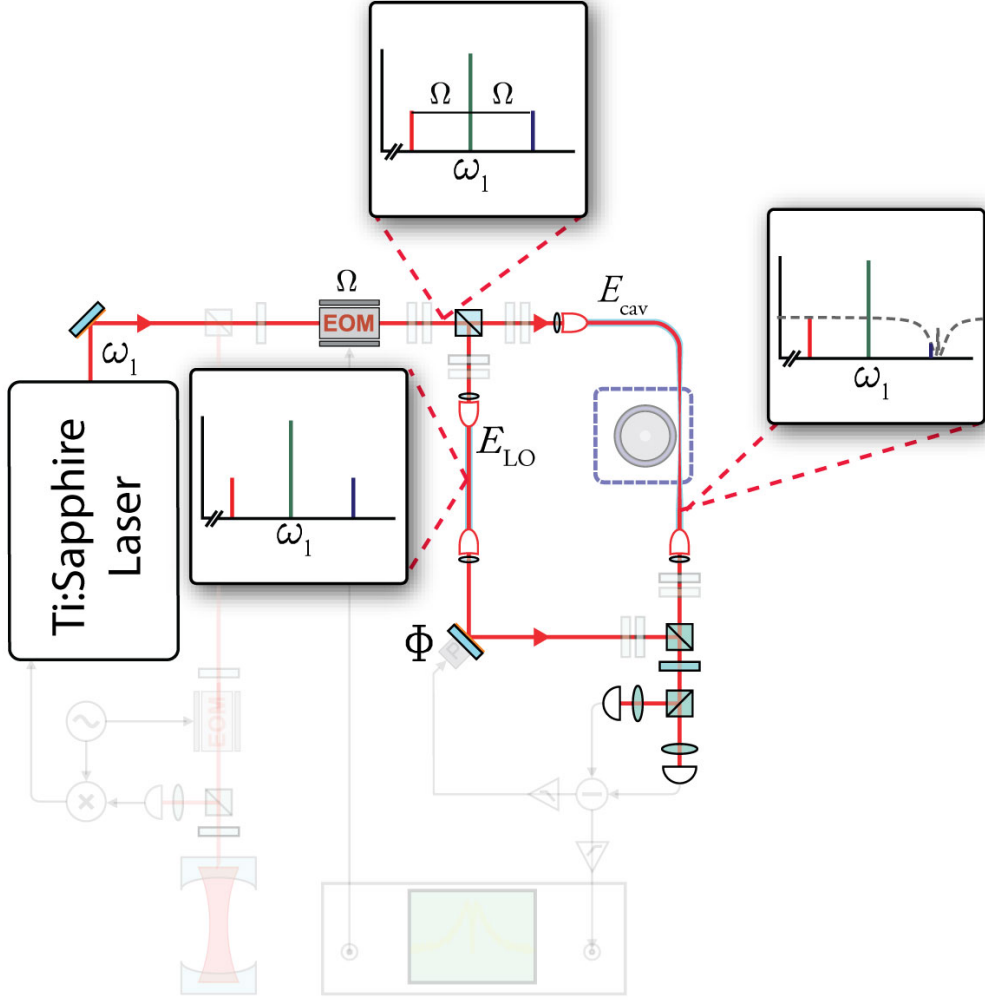$$B \approx -t''_{\text{us}} = -\text{Im}(t_p). \tag{S62}$$

FIG. S1: The optical setup as described in the main manuscript. The laser is phase modulated, creating two sidebands at frequency $\omega_l \pm \Omega$. The local oscillator field is transmitted unchanged whereas the field in the signal arm is affected by the cavity transmission. In the RSB regime, lower sideband and carrier, off resonant by approximately $2\Omega_m$ and Ω_m are not affected.

The complex amplitude response $t_{\text{hom}} = A + iB$ as measured on the network analyzer is hence given in good approximation by:

$$t_{\text{hom}} \approx 1 - t_p. \tag{S63}$$

The normalized response t'_{hom} is directly related to the normalized transmission $t_p{}'$:

$$t'_{\text{hom}} = \frac{t_{\text{hom}}}{1 - t_r} \tag{S64}$$

$$= 1 - t_p{}'. \tag{S65}$$

In particular, if we consider the form (S47) for the probe beam transmission, the measured signal is then given by:

$$t'_{\text{hom}} = \frac{\Gamma_m \kappa - 2i\Delta'\kappa}{\Omega_c^2 + \Gamma_m \kappa - 2i\Delta'\kappa}. \tag{S66}$$

We can easily calculate the normalized transmitted power:

$$|t'_{\mathrm{hom}}|^2 = 1 - \frac{\Omega_c^2/\kappa \left(\Omega_c^2/\kappa + 2\Gamma_m\right)}{\left(\Gamma_m + \Omega_c^2/\kappa\right)^2 + (2\Delta')^2} \tag{S67}$$

The measured signal is hence an inverted lorentzian peak with width Γ_{OMIT} (same width as $|t_p|^2$). The minimum value of the dip $|t'_{\mathrm{hom}}(\Delta' = 0)|^2$ can be linked very easily to the maximum value of the transmission window $|t'_p(\Delta' = 0)|^2$ by remarking that for $\Delta' = 0$ the transmission coefficients t_p and t_{hom} are real. The relation (S63) gives then:

$$|t'_{\mathrm{hom}}(\Delta' = 0)|^2 = \left(1 - \sqrt{|t'_p(\Delta' = 0)|^2}\right)^2 \tag{S68}$$

S 5. GROUP DELAY

EIT is the underlying phenomenon allowing for slowing down of light pulses. Indeed, the sharp transparency window in the medium is accompanied by a very abrupt change of its refractive index leading to slow group velocities (see [11] for a detailed analysis of the phenomenon). In the case of a single optically active element like an optomechanical device, the rapid phase dispersion $\phi(\omega) = \arg(t_p(\omega))$ leads to a 'group delay' τ_g given by:

$$\tau_g = -\frac{d\phi}{d\omega}. \tag{S69}$$

A full calculation based on the expression (S29) shows that the group delay diverges for small values of the transparency. However, in the regime $C \gtrsim 1$, where the medium is not completely opaque, a simple calculation based on expression (S47) is perfectly valid:

$$\phi(\Delta') = \arctan\left(\frac{2\Delta'\kappa}{\Omega_c + \Gamma_m\kappa}\right). \tag{S70}$$

This gives for the middle of the transparency window ($\Delta' = 0$):

$$\tau_g(\Delta' = 0) = \frac{2\kappa}{\Omega_c^2 + \Gamma_m\kappa} \tag{S71}$$

$$= \frac{1}{\Gamma_m}\left(\frac{2}{C+1}\right) \tag{S72}$$

$$= \frac{2}{\Gamma_{\mathrm{OMIT}}}. \tag{S73}$$

S 6. THEORETICAL TREATMENT OF A SPLITTED RESONANCE

Our rinf cavity can support two counterpropagating modes which are frequency degenerate for symmetry reasons. The propagation direction of the light in the coupling region therefore determines which mode is excited. However, as noted in early work on microspheres [14], and in theoretical as well as experimental work [15–17], due to residual scattering of light at the surface or in the bulk glass, the counterpropagating mode can also be significantly populated.

The essence of the phenomenon can be described by a coupled mode theory: if the two modes a_{cw} and a_{ccw} (see figure S2) are coupled by a coupling rate γ, the equations of motion become:

$$\dot{a}_{\mathrm{ccw}}(t) = (i(\Delta - g_0 x) - \kappa/2)a_{\mathrm{ccw}}(t) + i\frac{\gamma}{2}a_{\mathrm{cw}}(t) + \sqrt{\eta_c\kappa}s_{\mathrm{in}}(t) \tag{S74}$$

$$\dot{a}_{\mathrm{cw}}(t) = (i(\Delta - g_0 x) - \kappa/2)a_{\mathrm{cw}}(t) + i\frac{\gamma}{2}a_{\mathrm{ccw}}(t), \tag{S75}$$

and the radiation pressure force is now described by the equation:

$$\frac{d^2}{dt^2}x(t) + \Gamma_m\frac{d}{dt}x(t) + \Omega_m^2 x(t)+ = -\frac{\hbar g_0}{m_{\mathrm{eff}}}(|a_{\mathrm{ccw}}|^2 + |a_{\mathrm{cw}}|^2). \tag{S76}$$
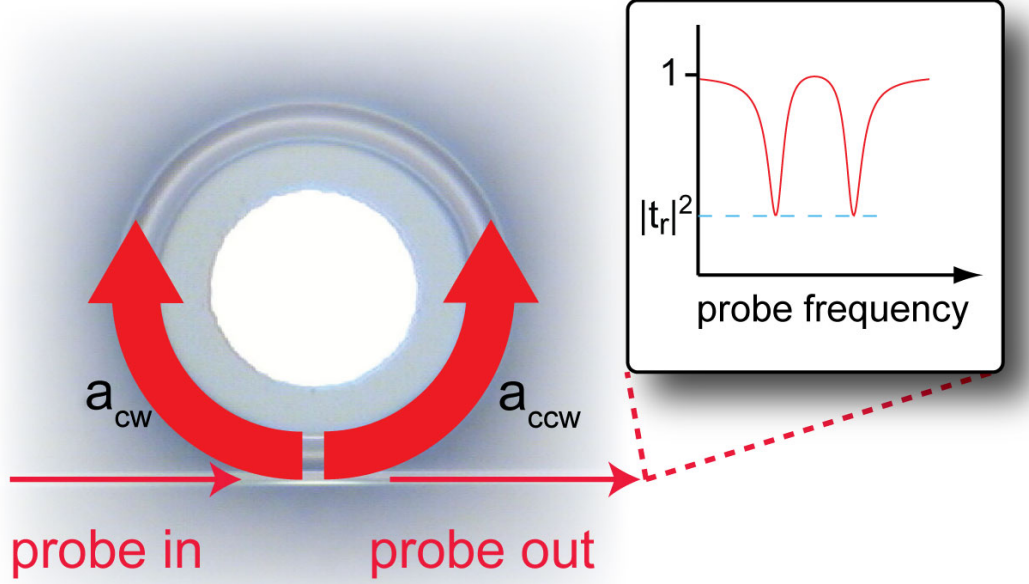
FIG. S2: In a ring cavity, two counterpropagating modes a_{cw} and a_{ccw} coexist. Only a_{ccw} is coupled to the waveguide, however, because of scattering into the counterpropagating mode, a_{cw} and a_{ccw} are coupled at a rate γ. For $\gamma \gg \kappa$, the transmission spectrum is a splitted resonance.

Indeed, because of the symmetry of the radial breathing mode, the oscillator is not driven by the cross term $2\mathrm{Re}(a_{\mathrm{ccw}}^* a_{\mathrm{cw}})$. We can then easily rewrite these equations in terms of the two stationary modes $a_+ = (a_{\mathrm{ccw}} + a_{\mathrm{cw}})/\sqrt{2}$ and $a_- = (a_{\mathrm{ccw}} - a_{\mathrm{cw}})/\sqrt{2}$:

$$\dot{a}_+(t) = \left[i(\Delta - g_0 x + \frac{\gamma}{2}) - \kappa/2 \right] a_+(t) + \sqrt{\frac{\eta_{\mathrm{c}}\kappa}{2}} s_{\mathrm{in}}(t) \tag{S77}$$

$$\dot{a}_-(t) = \left[i(\Delta - g_0 x - \frac{\gamma}{2}) - \kappa/2 \right] a_-(t) + \sqrt{\frac{\eta_{\mathrm{c}}\kappa}{2}} s_{\mathrm{in}}(t) \tag{S78}$$

$$\frac{d^2}{dt^2}x(t) + \Gamma_m \frac{d}{dt}x(t) + \Omega_m^2 x(t) = -\frac{\hbar g_0}{m_{\mathrm{eff}}}(|a_+|^2 + |a_-|^2). \tag{S79}$$

The two stationary modes are the eigenmodes of the evolution and the degeneracy is lifted by the coupling rate γ. In the limit $\gamma \gg \kappa$, the two modes are well resolved and only one of them (a_-) has to be considered since a_+ is non resonant and hence not populated. In this limit, the optomechanical system reads:

$$\dot{a}_-(t) = \left[i(\Delta - g_0 x - \frac{\gamma}{2}) - \kappa/2 \right] a_-(t) + \sqrt{\frac{\eta_{\mathrm{c}}\kappa}{2}} s_{\mathrm{in}}(t) \tag{S80}$$

$$\frac{d^2}{dt^2}x(t) + \Gamma_m \frac{d}{dt}x(t) + \Omega_m^2 x(t) = -\frac{\hbar g_0}{m_{\mathrm{eff}}}|a_-|^2. \tag{S81}$$

The system is perfectly equivalent to (S11)(S12) by formally replacing the coupling parameter η_{c} by $\eta_{\mathrm{c}}' \equiv \eta_{\mathrm{c}}/2$. This reduced 'effective coupling parameter' arises from the scattering of half of the intracavity power to the uncoupled mode a_{cw}.

With our present settings, we measured a residual transmission of $|t_r|^2 \approx 0.5$, we can hence infer the effective coupling parameter η_{c}' by solving

$$|t_r|^2 = 1/2 = (1 - 2\eta_{\mathrm{c}}')^2, \tag{S82}$$

leading to

$$\eta_c = \frac{2 - \sqrt{2}}{4} \approx 0.15. \tag{S83}$$

The intracavity power is hence smaller than the one calculated in the "standard" situation $\eta_c = 1/2$ and $\gamma = 0$. In the calculation of the coupling rate Ω_c, we took this factor into account; an additional reduction factor of 1.9 had to be introduced to account for taper losses in this experiment.

S 7.   TABLE OF SYMBOLS

symbol	meaning	definition
ω_l	laser frequency	
ω_c	cavity resonance frequency	
ω_p	probe frequency	
$\bar{\Delta}$	detuning of the control field	$\bar{\Delta} = \Delta - g_0 \bar{x}$
κ	optical linewidth (FWHM)	
κ_0	intrinsic loss rate	
κ_{ex}	coupling rate to the waveguide	
η_{c}	coupling parameter	$\eta_{\mathrm{c}} = \kappa_{\mathrm{ex}}/(\kappa_0 + \kappa_{\mathrm{ex}})$
$\bar{a}$	mean intracavity mode amplitude	
$\bar{s}_{\mathrm{in}}$	mean drive amplitude	
g_0	optomechanical coupling	$d\omega'_{\mathrm{c}}/dx$
Ω_m	mechanical resonance frequency	
Γ_m	mechanical damping rate	
m_{eff}	effective mass	
$\bar{x}$	equilibrium displacement	
Δ'	detuning of the probe from the center of the OMIT feature	$\Delta' = \omega_p - \omega_l - \Omega_m$
x_{zpf}	zero-point fluctuations	$x_{\mathrm{zpf}} = \sqrt{\hbar/(2m_{\mathrm{eff}}\omega_m)}$
Ω_c	optomechanical coupling rate	$\Omega_c = 2g_0 \bar{a} x_{\mathrm{zpf}}$
C	cooperativity	$C = \Omega_c^2/(\Gamma_m \kappa)$
$\chi(\Omega)$	mechanical susceptibility	$\chi(\Omega) = (m_{\mathrm{eff}}(\Omega_{\mathrm{m}}^2 - \Omega^2 - i\Gamma_{\mathrm{m}}\Omega))^{-1}$
t_p	complex amplitude transmission at probe frequency	
t_{hom}	complex transmission signal measured in the homodyne receiver	
β	Modulation depth	
t_{us}	complex transmission of the upper sideband	
t_{c}	complex transmission of the carrier	
t_{ls}	complex transmission of the lower sideband	
a_{cw}	amplitude of the clockwise propagating mode	
a_{ccw}	amplitude of the counterclockwise propagating mode	
γ	coupling between the two counter propagating modes	
a_+	symmetric stationary mode	$a_+ = (a_{\mathrm{cw}} + a_{\mathrm{ccw}})/\sqrt{2}$
a_-	antisymmetric stationary mode	$a_- = (a_{\mathrm{cw}} - a_{\mathrm{ccw}})/\sqrt{2}$

[1] A. Schliesser. *Cavity Optomechanics and Optical Frequency Comb Generation with Silica Whispering-Gallery-Mode Microresonators.* PhD thesis, Ludwig-Maximilians-Universität München, 2009. http://edoc.ub.uni-muenchen.de/10940/, page 121ff.

[2] A. Schliesser and T. J. Kippenberg. Cavity optomechanics with silica microresonators. In E. Arimondo, P. Berman, and C. C. Lin, editors, *Advances in atomic, molecular and optical physics*, volume 58. Elsevier Academic Press, 2010. (in print, preprint at arXiv:1003.5922).

[3] G. S. Agarwal and S. Huang. Electromagnetically induced transparency in mechanical effects of light. *Physical Review A*, 81:041803, 2010.

[4] C. K. Law. Interaction between a moving mirror and radiation pressure: A Hamiltonian formulation. *Physical Review A*, 51:2537–2541, 1995.

[5] M. Cai, O. Painter, and K. J. Vahala. Observation of critical coupling in a fiber taper to a silica-microsphere whispering-gallery mode system. *Physical Review Letters*, 85(1):74–77, 2000.

[6] S. M. Spillane, T. J. Kippenberg, O. J. Painter, and K. J. Vahala. Ideality in a fiber-taper-coupled microresonator system for application to cavity quantum electrodynamics. *Physical Review Letters*, 91(4):043902, 2003.

[7] C. Fabre, M. Pinard, S. Bourzeix, A. Heidmann, E. Giacobino, and S. Reynaud. Quantum-noise reduction using a cavity with a movable mirror. *Physical Review A*, 49:1337–1343, 1994.

[8] A. Dorsel, J. D. McCullen, P. Meystre, E. Vignes, and H. Walther. Optical bistability and mirror confinement induced by radiation pressure. *Physical Review Letters*, 51(17):1550–1553, 1983.

[9] C. W. Gardiner and P. Zoller. *Quantum Noise.* Springer, 2004.

[10] I. Wilson-Rae, N. Nooshi, W. Zwerger, and T. J. Kippenberg. Theory of ground state cooling of a mechanical oscillator using dynamical backaction. *Physical Review Letters*, 99(9):093901, 2007.

[11] P. W. Milonni. *Fast light, slow light and left-handed light.* Taylor and Francis, 2005.

[12] M. O. Scully and M. S. Zubairy. *Quantum Optics.* Cambridge University Press, 1997.

[13] H. J. Kimble. Structure and dynamics in cavity quantum electrodynamics. In P. R. Berman, editor, *Cavity Quantum Electrodynamics*, Advances in Atomic, Molecular and Optical Physics. Academic Press, 1994.

[14] D. S. Weiss, V. Sandoghdar, J. Hare, V. Lefévre-Seguin, J. M. Raimond, and S. Haroche. Splitting of high-Q Mie modes induced by light backscattering in silica microspheres. *Optics Letters*, 20(18):1835–1837, 1995.

[15] M. L. Gorodetsky, A. D. Pryamikov, and V. S. Ilchenko. Rayleigh scattering in high-Q microspheres. *Journal of the optical society of America B - Optical physics*, 17(6):1051–1057, 2000.

[16] T. J. Kippenberg, S. M. Spillane, and K. J. Vahala. Modal coupling in traveling-wave resonators. *Optics Letters*, 27(19):1669–1671, 2002.

[17] A. Mazzei, S. Götzinger, L. de S. Menezes, G. Zumofen, O. Benson, and V. Sandoghdar. Controlled coupling of counterpropagating whispering-gallery modes by a single Rayleigh scatterer: a classical problem in a quantum optical light. *Physical Review Letters*, 99:173603, 2007.